Supplementary Information

A First-Principles Study on the Multilayer Graphene Nanosheets Anode Performance for Boron-Ion Battery

Mustapha Umar [1], Chidera C. Nnadiekwe [1], Muhammad Haroon [1], Ismail Abdulazeez [2,*], Khalid Alhooshani [1,3], Abdulaziz A. Al-Saadi [1,3] and Qing Peng [4,5,6,*]

[1] Chemistry Department, King Fahd University of Petroleum and Minerals, Dhahran 31261, Saudi Arabia; g201708770@kfupm.edu.sa (M.U.); g201707330@kfupm.edu.sa (C.C.N.); muhammad.hanif@kfupm.edu.sa (M.H.); hooshani@kfupm.edu.sa (K.A.); asaadi@kfupm.edu.sa (A.A.A.-S.)

[2] Interdisciplinary Research Center for Membranes and Water Security, King Fahd University of Petroleum and Minerals, Dhahran 31261, Saudi Arabia

[3] Interdisciplinary Research Center for Refining and Advanced Chemicals, King Fahd University of Petroleum and Minerals, Dhahran 31261, Saudi Arabia

[4] Interdisciplinary Research Center for Hydrogen and Energy Storage, King Fahd University of Petroleum and Minerals, Dhahran 31261, Saudi Arabia

[5] Physics Department, King Fahd University of Petroleum and Minerals, Dhahran 31261, Saudi Arabia

[6] KACARE Energy Research and Innovation Center at Dhahran, Dhahran 31261, Saudi Arabia

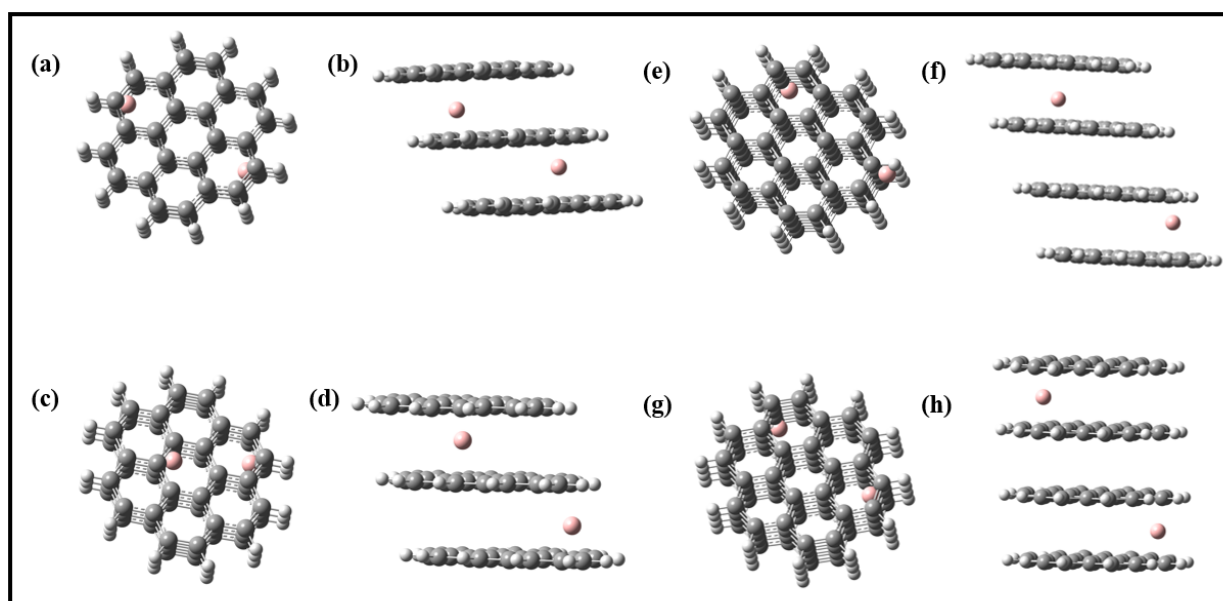[*] Correspondence: ismail.abdulazeez@kfupm.edu.sa (I.A.); qing.peng@kfupm.edu.sa (Q.P.)

Figure S1. Optimized structures of **(a)** and **(b)** 2B@TG (side and topviews), **(c)** and **(d)** 2B@TG (side and topviews), **(e)** and **(f)** $2B^{3+}$@TTG (side and topviews), **(g)** and **(h)** $2B^{3+}$@TTG (side and topviews).
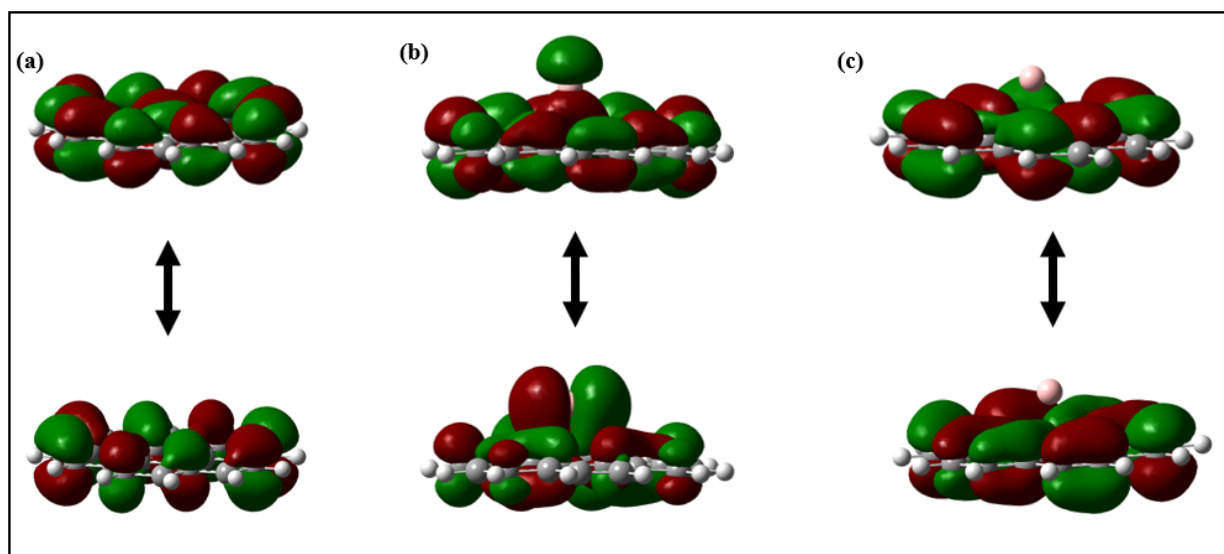
Figure S2. Molecular Orbital HOMO (Lower) and LUMO (upper) of (a) Monolayer Graphene Sheet (MG), (b) B@MG, (c) B^{3+}@MG.
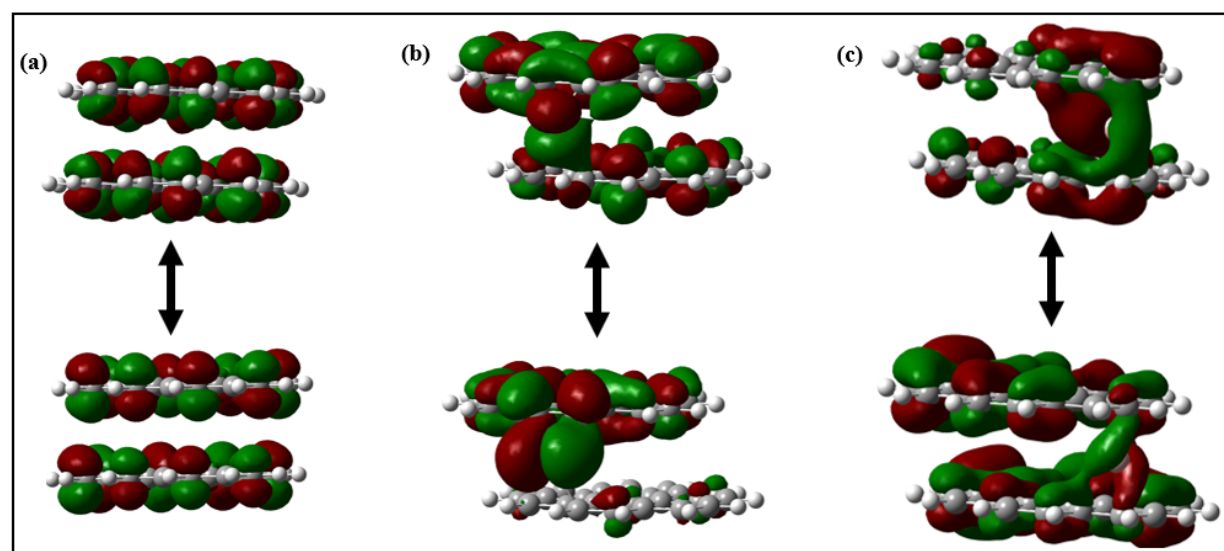

Figure S3. Molecular Orbital HOMO (Lower) and LUMO (upper) of (a) Bilayer Graphene Sheet (BG) (b) B@BG, (c) B^{3+}@BG.
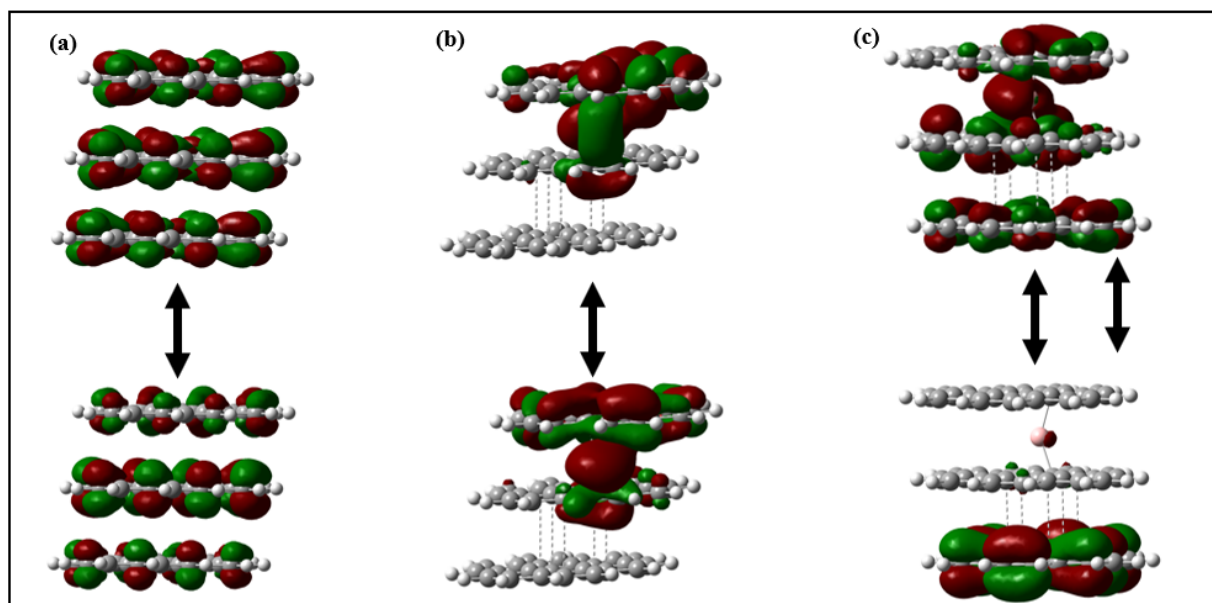
Figure S4. Molecular Orbital HOMO (Lower) and LUMO (upper) of (a) Trilayer Graphene Sheet (TG), (b) B@TG, (c) B^{3+}@TG.
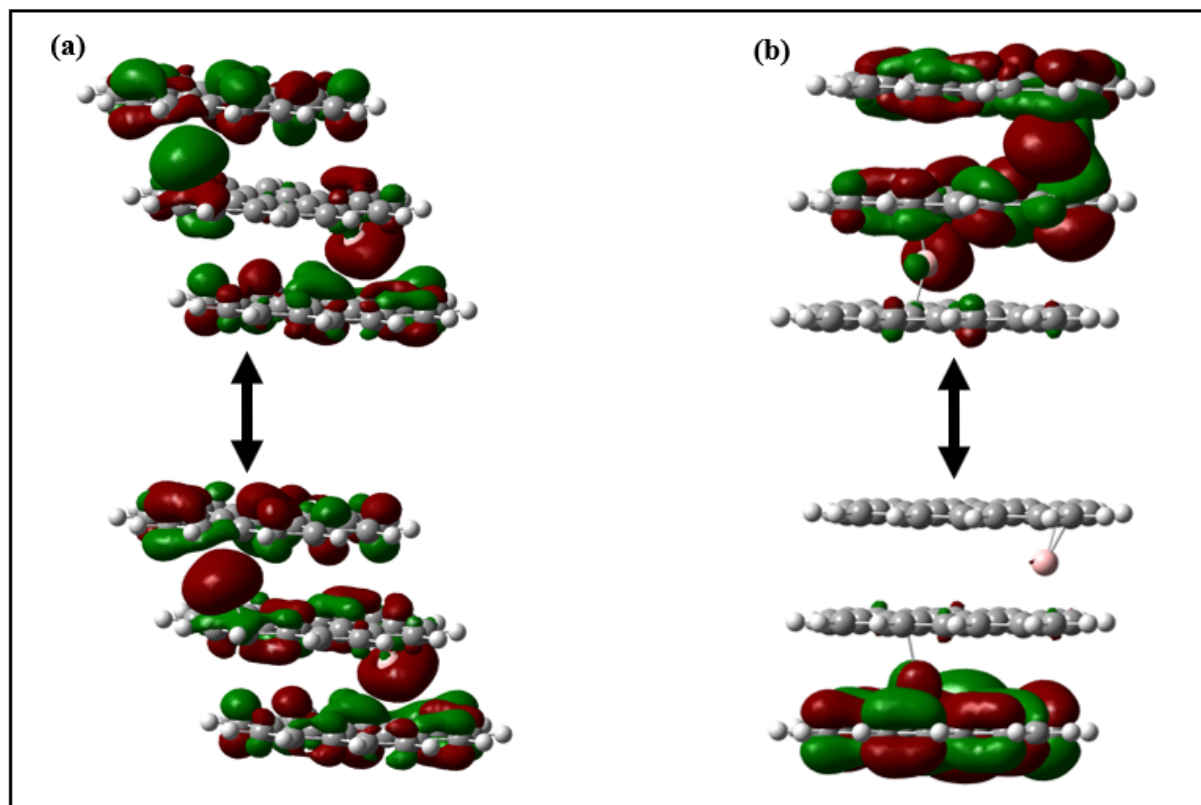

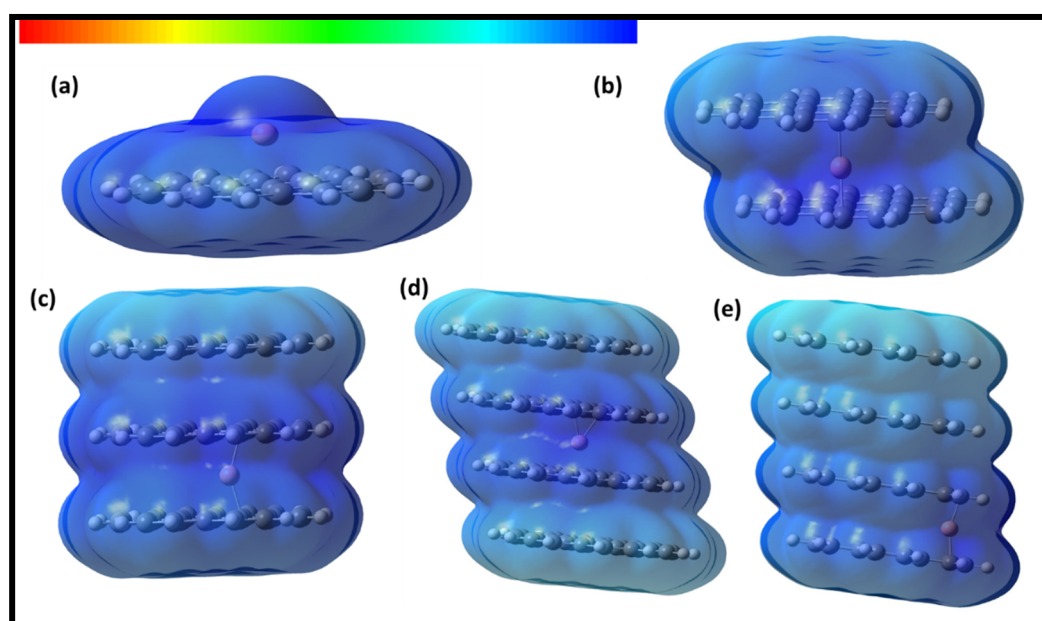**Figure S5.** Molecular Orbital HOMO (Lower) and LUMO (upper) of (a) 2B@TG and (b) 2B^{3+}@TG.

Figure S6. Electrostatic potential (ESP) map of (a) B^{3+}@MG, (b) B^{3+}@BG, (c) B^{3+}@TG, (d) B^{3+}@TTG_sym and (d) B^{3+}@TTG_asym.
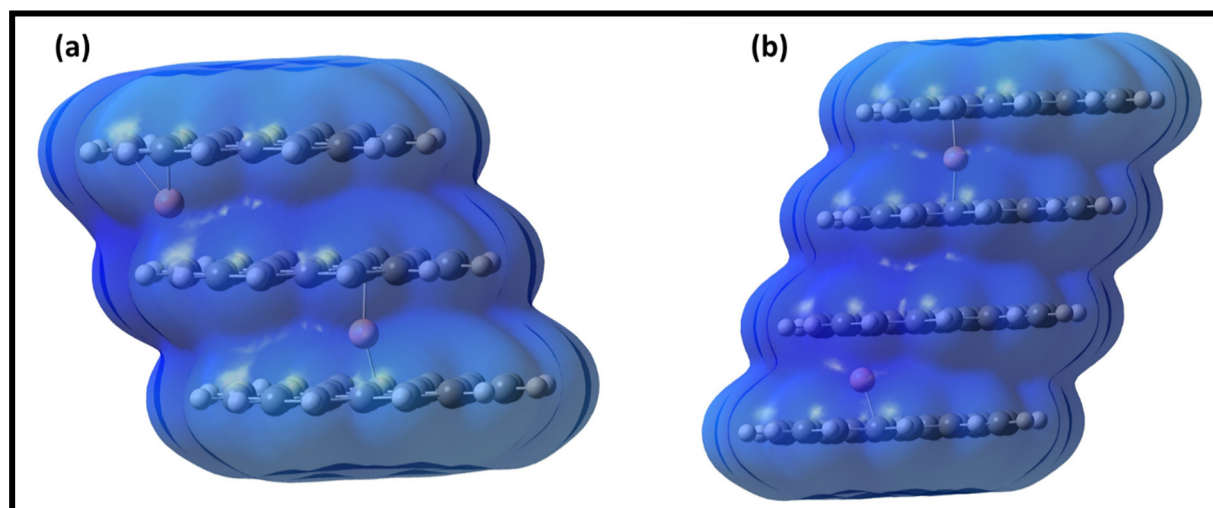

Figure S7. Electrostatic potential (ESP) (a) $2B^{3+}$@TG and (b) $2B^{3+}$@TTG.

Figure S8. The reduced density gradient (RDG) isosurfaces analyses of (**a**), (**b**) and (**c**) **2**B³⁺@TG (complex and RDG), and (**d**), (**e**) and (**f**) **2**B³⁺@TTG (complex and RDG). Where blue regions correspond to strong hydrogen bonds; red regions indicate strong steric effects, whereas green regions describe strong van der Waals interactions.
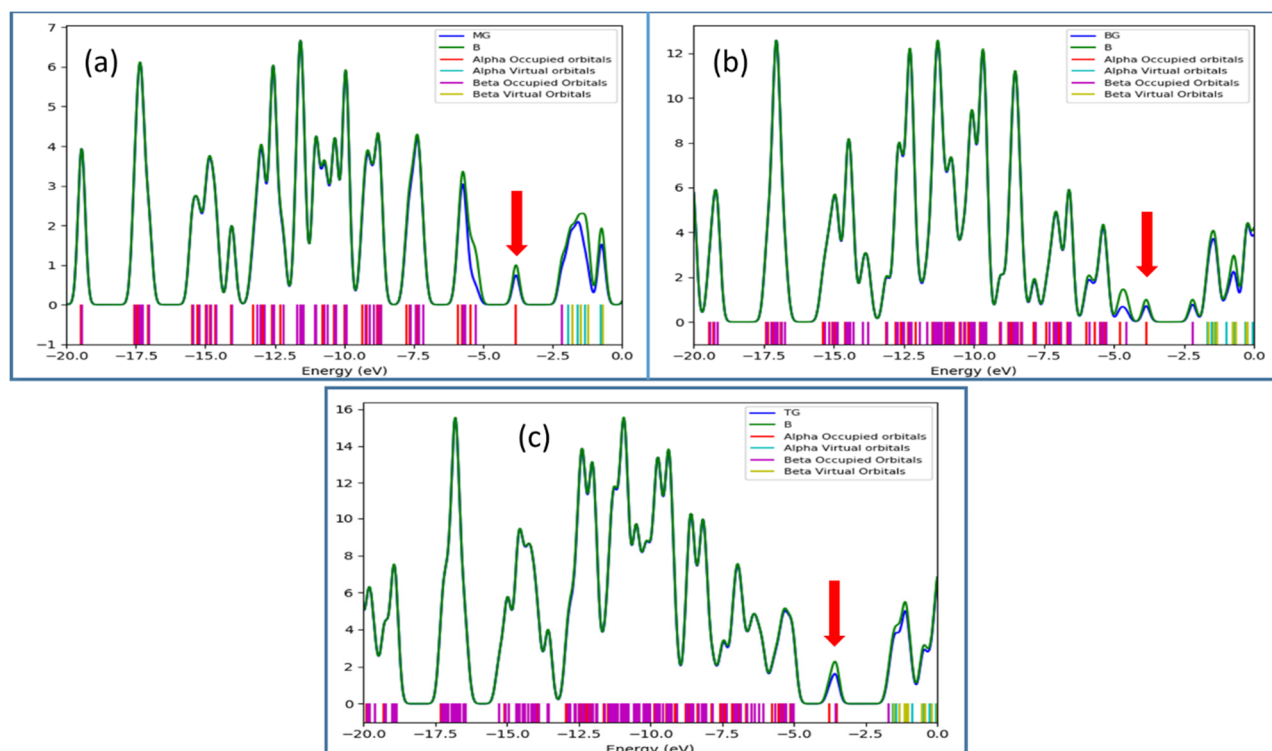

Figure S9. Partial density of states (PDOS) plots (a) B@MG (b) B@BG and (c) B@TG.
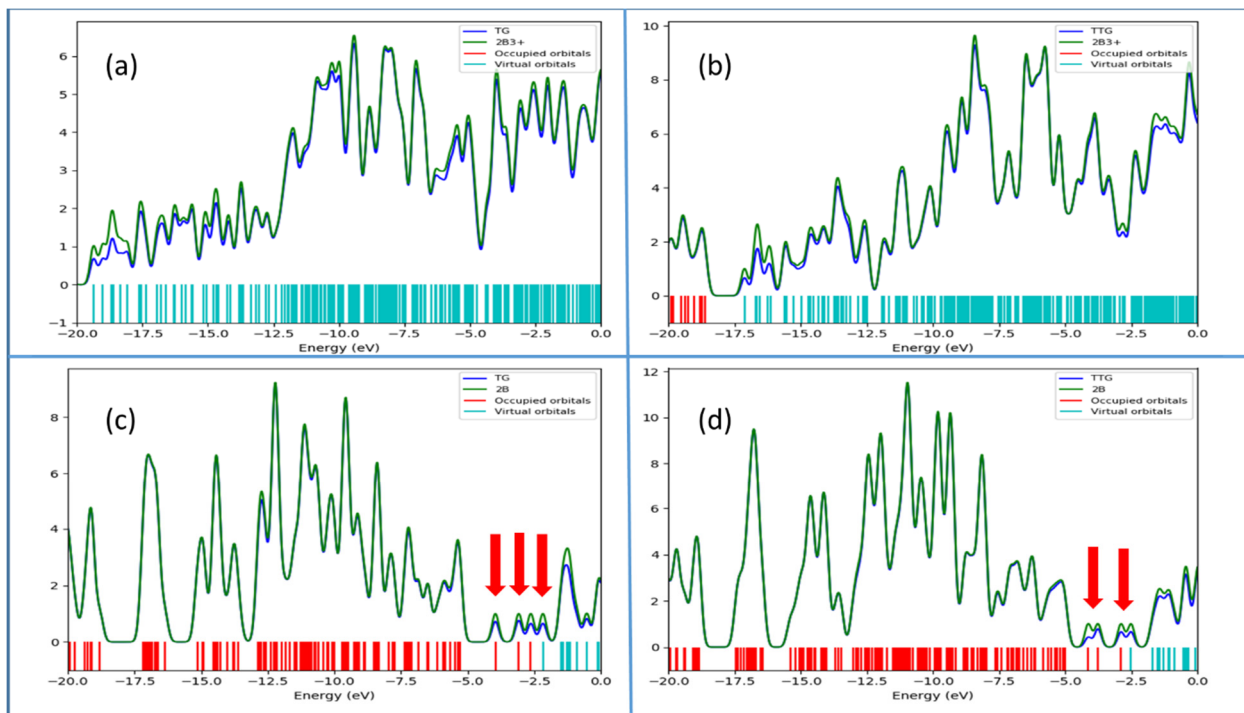
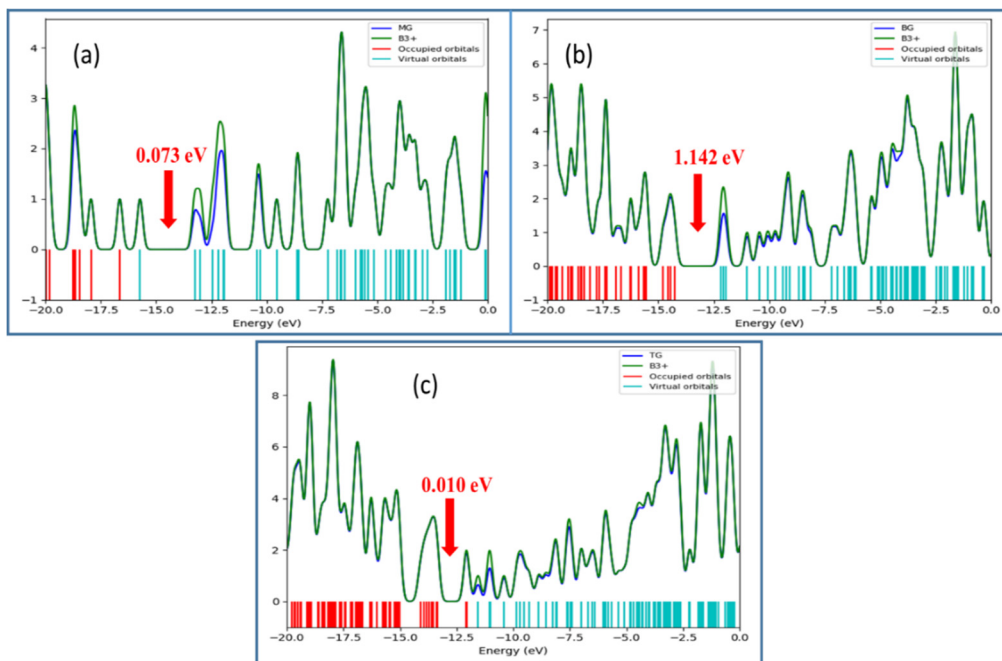**Figure S10.** Partial density of states (PDOS) plots (a) 2B³⁺@TG (b) 2B³⁺@TTG (c) B@TG_sym and (d) 2B@TTG.

Figure S11. Partial density of states (PDOS) plots of (a) B³⁺@MG (b) B³⁺@BG and (c) B³⁺@TG.

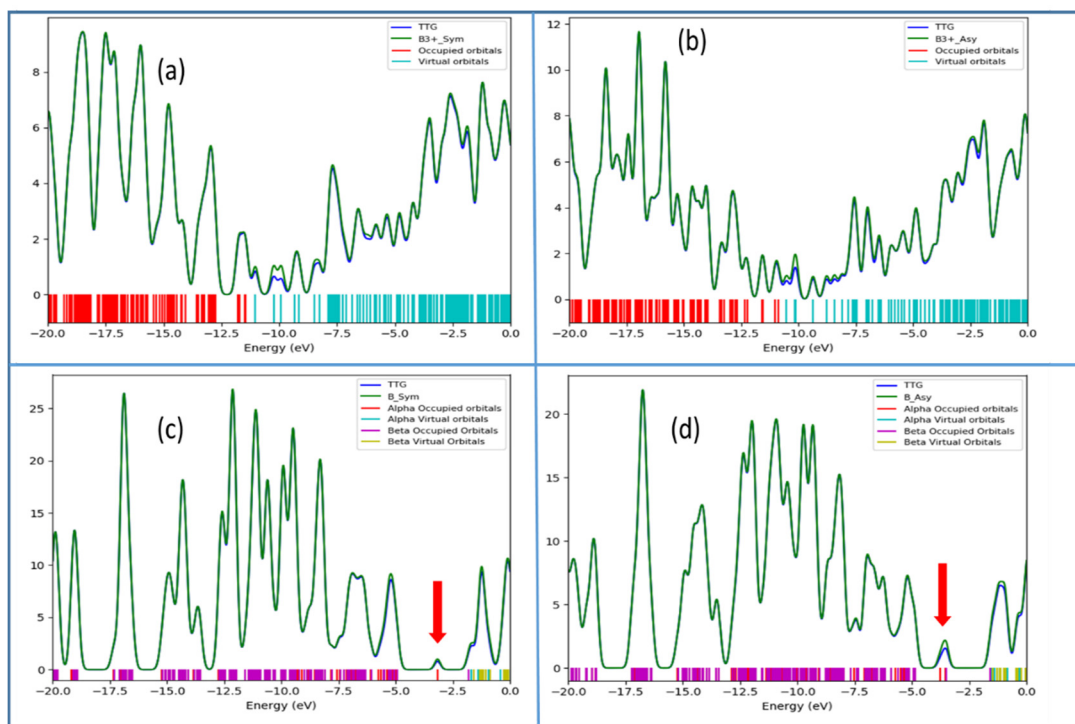**Figure S12.** Partial density of states (PDOS) plots of (a) B³⁺@TTG_sym (b) B³⁺@TTG_asym (c) B@TTG_sym and (d) B@TTG_asym.
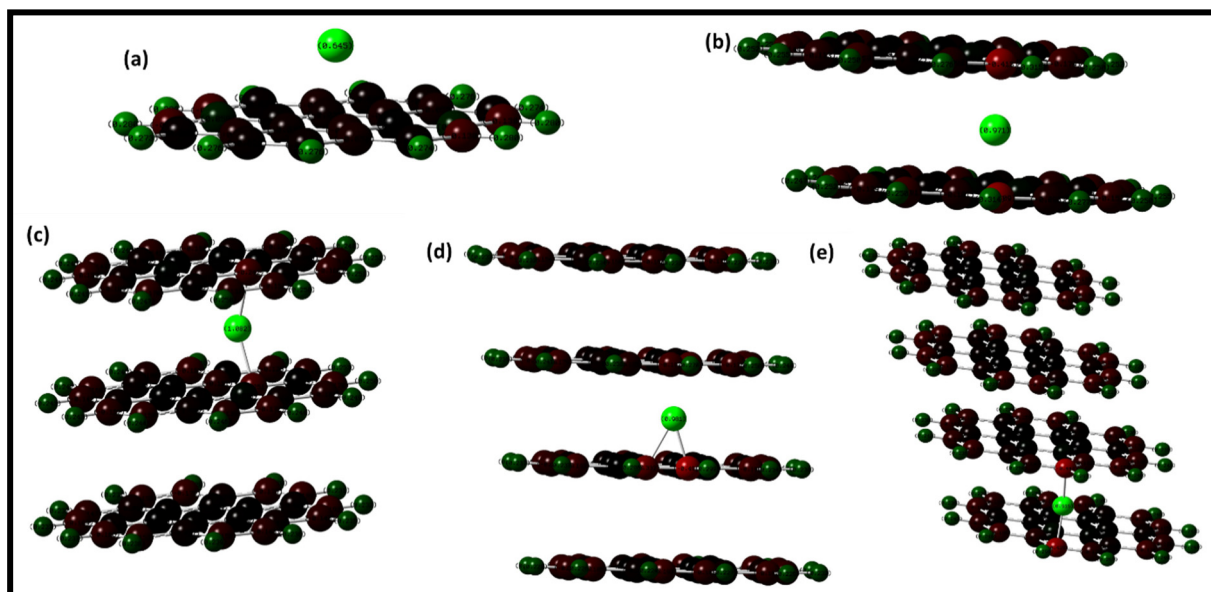

Figure S13. Natural bond orbital charges of (a) B³⁺@MG, (b) B³⁺@BG and (c) B³⁺@TG, (d) B³⁺@TTG_sym and (e) B³⁺@TTG_asym.
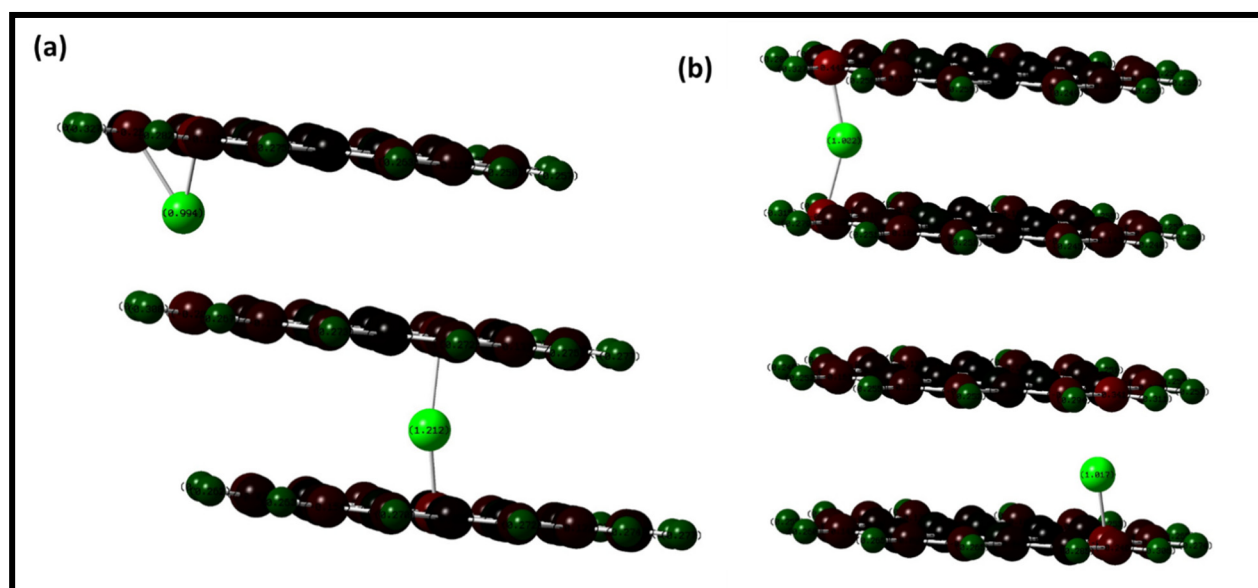
Figure S14. Natural bond orbital charges of (a) 2B^{3+}@TG and (b) 2B^{3+}@TTG.

Table S1. Electronic properties.

Complexes	E$_{HOMO}$ (eV)	E$_{LUMO}$ (eV)	E$_g$ (eV)	μ (eV)	η (eV)	χ(eV)	E$_a$ (eV)
MG	−5.085	−2.242	2.843	13.42	1.421	3.663	2.242
BG	−4.883	−2.249	2.635	12.72	1.317	3.566	2.249
TG	−4.760	−2.233	2.527	12.23	1.264	3.496	2.233
FGS	−4.622	−2.151	2.472	11.47	1.236	3.386	2.151
B@MG	−4.857	−3.125	1.731	15.93	0.866	3.991	3.125
B^{3+}@MG	−16.31	−16.23	0.073	264.7	0.036	16.27	16.23
B@BG	−4.240	−3.122	1.118	13.55	0.559	3.681	3.122
B^{3+}@BG	−13.98	−12.84	1.142	179.8	0.571	13.41	12.84
B@TG	−3.407	−2.614	0.793	9.061	0.396	3.010	2.614
B^{3+}@TG	−11.96	−11.97	0.010	143.1	−0.005	11.96	11.97
B@TTG_asym	−3.347	−2.507	0.840	8.567	0.420	2.927	2.507
B^{3+}@TTG_asym	−10.85	−10.84	0.010	117.5	0.005	10.84	10.84
B@TTG_sym	−4.688	−2.680	2.009	13.57	1.004	3.684	2.680
B^{3+}@TTG_sym	−11.28	−11.28	0.003	127.1	0.002	11.28	11.28
2B@TG	−2.862	−2.787	0.075	7.979	0.038	2.825	2.787
2B^{3+}@TG	−20.08	−19.84	0.241	398.4	0.121	19.96	19.84
2B@TTG	−3.099	−3.059	0.040	9.479	0.020	3.079	3.059
2B^{3+}@TTG	−18.33	−17.66	0.672	323.9	0.336	18.0	17.66